THE JOURNAL OF PHYSICAL CHEMISTRY B

Article

pubs.acs.org/JPCB

Probing Ligand-Binding Modes and Binding Mechanisms of Benzoxazole-Based Amide Inhibitors with Soluble Epoxide Hydrolase by Molecular Docking and Molecular Dynamics Simulation

Hang Chen, Ying Zhang, Liang Li, and Ju-Guang Han*

National Synchrotron Radiation Laboratory, University of Science and Technology of China, Hefei 230029, People's Republic of China

Supporting Information

ABSTRACT: Soluble epoxide hydrolase (sEH) has become a new therapeutic target for treating a variety of human diseases. The inhibition of human sEH hydrolase activity was studied by molecular docking and molecular dynamics (MD) simulation techniques. A set of six benzoxazole-based amide inhibitors binding to sEH has been studied through molecular docking, MD simulation, free energy calculations, and energy decomposition analysis. On the basis of molecular mechanics-generalized Born/surface area (MM-GB/SA) computation and normal-mode analysis (NMA), the obtained results indicate that the rank of calculated binding free energies ($\Delta\Delta G_{TOT}$) of these inhibitors is in excellent agreement with that of experimental bioactivity data (IC_{50}). The correlation coefficient (r^2) between the predicted $\Delta\Delta G_{TOT}$ and IC_{50} is 0.88. van der Waals energies are the largest component of the total energies, and the entropy changes play an indispensable role in determining the $\Delta\Delta G_{TOT}$. Rational binding modes were discussed and determined by the docking results and binding free energies. The free energy decomposition of each residue reveals that the residue Trp334 dominates the most binding free energies among all residues and that the activities for these molecules to the sEH are not decided by hydrogen bonds or a certain residue but by the common effect of multiple side chains in the active site.

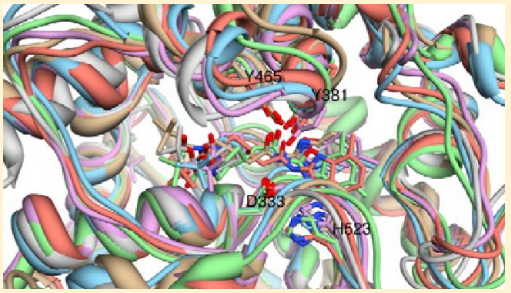

1. INTRODUCTION

Soluble epoxide hydrolase (sEH) has a widespread distribution in mammalian tissues such as liver, kidney, intestine, and vascular tissue.[1] It is an enzyme responsible for the conversion of epoxides to the corresponding vicinal diols by the addition of a water molecule. The primary endogenous substrates of sEH are four epoxyeicosatrienoic acid regioisomers (EETs) produced from arachidonic acid by cytochrome P450 epoxygenses.[1,2] An increasing number of evidence have demonstrated the concept that EETs play a critical role in significant physiological effects such as reduced blood pressure,[3] anti-inflammatory,[4,5] neuroprotective,[6] antiapoptotic effects,[7] and cardioprotective effects.[8−10] However, many pathways of EETs metabolism may decrease the in vivo concentration of EETs, resulting in several disease states. The primary pathway of EETs metabolism is through hydration by the sEH enzyme,[11] which converts EETs to the corresponding dihydroxyeicosatrienoic acids (DHETs).[12,13] It is generally believed that DHETs are inactivation products of EETs[14,15] and that they diminish biological activity in many systems. Hence, an efficient approach is to inhibit EET hydrolysis and increase the in vivo concentration of EETs and enhance their beneficial effects.[16] Several published research works indicate that sEH has become a potential pharmacological target for hypertension, inflammation, organ-protection, heart failure, and cardiovascular diseases.[16−20]

In the past few years, considerable research efforts have been dedicated to develop sEH inhibitors as prospective drugs for the prevention and treatment of multiple disease states.[16,21−25] Numerous potent sEH inhibitors have been disclosed in published and patent literature.[24,26−28] Various compounds such as urea derivatives, amides, chalcone oxides, carbamates, acyl hydrazones, and other pharmacophores have been explored as sEH inhibitor. Most of these compounds include a urea or amide moiety to mimic the activation of the endogenous epoxide EETs. However, it is still a significant challenge to improve inhibitors with high potency, solubility, good pharmacokinetics, and selectivity against other biological targets. So far, the only inhibitor AR9281 had been conducted in clinical trials as a sEH inhibitor.[16,29] Hence, developing new, rational, secure, and potent selective inhibitors has great significance and potential application.

Recently, Li et al. have designed and tested a series of novel, potent organic compounds as sEH inhibitors by structure-based virtual screening.[30] The structures of six complexes selected here are listed in Table 1. Li et al. predicted and analyzed the binding modes and the affects of diverse substituted positions on benzoxazole ring according to molecular docking results. At the atomic level, understanding this class of small molecule

Received: May 15, 2012
Revised: July 12, 2012
Published: August 2, 2012

Table 1. Structures of Lead Compound and Six Compounds Studied in This Work

group A	structure	IC50(nM)	group B	structure
lead compound	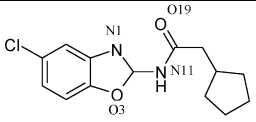	32		
1api	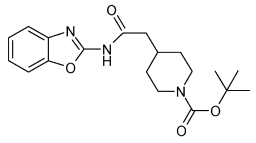	94.3	1a	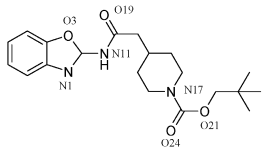
1bpi	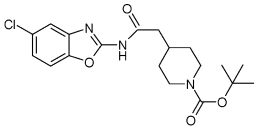	6.92	1b	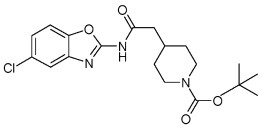
1cpi	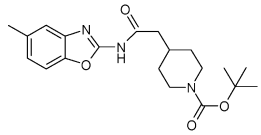	11.4	1c	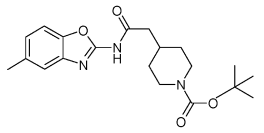
1dpi	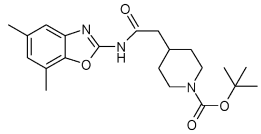	73	1d	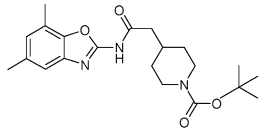
1epi	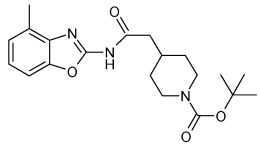	272	1e	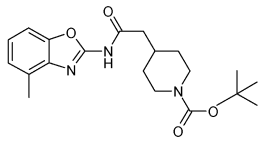
1fpi	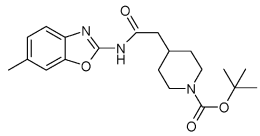	202	1f	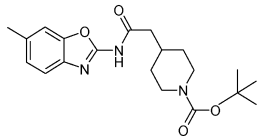

interaction with protein may promote the development of sEH inhibitors with better potency. However, a detailed mechanism of both energy and structure remains largely unknown. We are interested in the inhibition model for each molecule and how these benzoxazole-based amide inhibitors interact with sEH.

However, with the development of experimental techniques (such as X-ray crystallography and NMR) and improving computational efficiency and techniques, computational method in structure-based drug design has been successfully applied in many drug discovery projects.[31,32] In addition, since the prediction of the binding mode of ligand to receptor, protein−ligand interaction, binding free energy, and the rank of the ligands of potential pharmacophore are the necessary steps in the process of structure-based drug design and lead optimization, selection of fast and accurate methods and tools is of vital importance for designed compounds prior to synthesis. Molecular docking can be applied to scan large compound libraries and predict the binding mode of a protein−ligand complex due to its advantage of rapidity and inexpensiveness. However, its accuracy of predicting binding free energy and scoring functions should be improved. Molecular dynamics simulation as an essential tool for studying biological macromolecules can calculate binding free energy and predict the biological activity of compounds by combining molecular dynamics simulation with MM-GB/SA method and rapidly refine docking results. At the same time, it also can explore the dynamic properties of protein−ligand complex. It has been reported that the computational protocol combining molecular docking and molecular dynamics simulation is reliable and accurate for predicting protein−ligand binding mode and binding free energy.[33−35]

In present work, our goal is to probe the binding modes between sEH and inhibitors described in Li's work[30] and explain the inhibitor−residue interactions. Molecular docking and molecular dynamics simulation were applied as a computational strategy to gain insight into the binding modes of this class of compounds and further identify the key residues for ligand binding. The results obtained can provide some meaningful clues in the future design of highly potent sEH inhibitors.

2. MATERIALS AND COMPUTATIONAL METHODS

2.1. System Setups. The starting structure of sEH protein is obtained from the crystal structure (PDB entry 3PDC), which includes a C-terminal domain with epoxide hydrolase activity. All crystal water molecules and bound inhibitor (lead compound) were removed from the PDB file. In order to improve the computational efficiency, only chain A was extracted from the crystal structure. Detailed discussions about replacing the homodimer with one of two monomer subunits can be found in the Supporting Information. Six representative inhibitors were taken from Li's paper[30] and their

dx.doi.org/10.1021/jp304736e | J. Phys. Chem. B 2012, 116, 10219−10233

chemical structures are shown in Table 1. All of them share a common structure and their names are kept the same as those in Li's paper.[30] Among these ligands, lead compound is the only solved crystal structure binding upon sEH. On the basis of the lead compound, a series of amide-like inhibitors with a benzoxazole template linked to the amide moiety was designed by Li et al.[30] JME Molecular Editor[36] was used to sketch the structures of these inhibitors, and then, they were converted into 3D representations by the PRODRG server.[37] In order to get the most stable conformations, all the 3D structures of the ligands were fully optimized at the B3LYP/6-31G(d, p) level by the Gaussion03 program.[38] Finial structures were used for molecular docking using AutoDock 4.2.[39]

2.2. Parameters Setup for Molecular Docking. Before docking calculation, the lead compound was first removed from the crystal structure and the structure of sEH was then used as the receptor for the following docking experiment. Some previous studies showed that the catalytic pocket, regardless of whether it is occupied by a urea inhibitor, is rigid in general.[40−43] Hence, rigid-receptor docking approach was employed on receptor conformation, while all the torsional bonds of those ligands were set free. AutodockTools 1.5.4[44] was used to prepare the PDBQT file for the receptor and ligands. Meanwhile, during PDBQT file preparation, all hydrogen atoms were added, Gasteiger charges were assigned, and rotatable bonds were identified.

For the AutoGrid[45] calculation, grid module was employed to create grid maps with 70 × 70 × 70 points of 0.375 Å spacing. The center of the box was set in the centroid of the inhibitor. For the AutoDock[45] calculation, Lamarckian genetic algorithm was used for the receptor and ligand docking with the following settings of parameters: population size of individuals 150, a maximum number of 25 million energy evaluations, a maximum number of generations of 27 000, a mutation rate of 0.02, a crossover rate of 0.8, and an elitism value of 1 were set up. All other docking parameters were set to default. Fifty independent docking runs were conducted for each docking calculation. The docked conformations were clustered according to a root-mean-square deviation (rmsd) within a criterion of 2 Å and evaluated depending on the binding free energies.

In order to verify whether the program could reproduce ligand conformation elucidated in the crystallographic structure, we extracted the lead compound out of the crystal structure, and then, a molecular docking was carried out using the docking parameters mentioned above. Afterward docking experiment, 50 independent runs were obtained. The docked conformations were analyzed by examining their relative total energy scores, rmsd clustering, and hydrogen bond distances. The best docked conformation was determined by the size of clusters according to the obtained rmsd, the estimated binding energies and hydrogen bonds formed between the amide moiety of the inhibitor and the residues (Tyr381 or Tyr465 and Asp333) of the sEH active site within a distance of 2.8 Å. Among several similar docking poses, the more energetically favorable conformation was selected. The superimposition of the lead compound between crystal structure and docking conformation was shown in Figure 1.[46] It shows that the two structures are almost identical in the binding pocket, suggesting that the docking algorithm is reliably used to predict the binding conformation for this system.

For the other six inhibitors (listed in Table 1), the same parameters and criterions were applied to dock ligand into receptor and select the final products. The initial position and orientation of the ligand were kept referring to the binding mode of lead compound in X-ray crystallographic structure.[47] The final structures selected from docking result were used as starting structures for the following MD simulations.

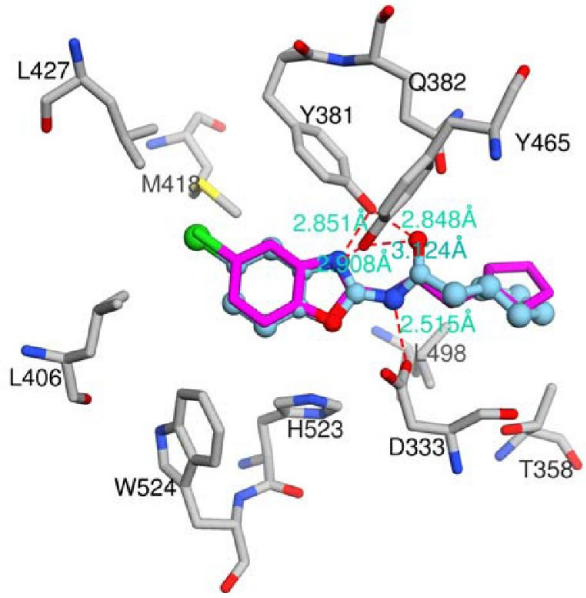

Figure 1. Conformation of sEH/lead compound complex in sEH protein active site. For the docking conformation, the lead compound is shown as a ball and stick model. For the crystal structure, the lead compound is shown as a magenta stick model. The residues of sEH are shown in a light gray stick model. Hydrogen bonds are displayed in red dashed lines with the corresponding distances. For clarity, the hydrogen atoms are omitted. The figure is created by using Chimera software.[46]

2.3. Parameters Setup for MD Simulations. All MD simulations were carried out using the AMBER10 suite[48] with the FF03 force field[49,50] in this study. The crystal structure and the best docking results were used as the initial binding conformations for MD simulation. For ligands, hydrogen atoms and AM1-BCC charges were added using ANTECHAMBER, while the missing atoms of the sEH protein were added using the TLEAP program in the AMBER10 software package.[48] The PARMCHECK program was used to obtain General AMBER Force Field (GAFF)[51] parameters for the ligands. All ionizable residues, except residue His523, were set at default protonation states at a neutral pH by TLEAP.[48] To find what the most possible protonation state is, three possible protonation states of histidine (Hie523, Hid523, and Hip523) located in the active site were considered, respectively. All selected complexes were solvated in an octahedron periodic box of TIP3P[52] water molecules with a margin of 8 Å along each dimension. The net negative charge of system was neutralized by adding an appropriate number of counter Na^+ ions.

Prior to MD simulations, the entire system was minimized by two steps, each of which consists of 10 000 cycles (5000 cycles of steepest descent and 5000 cycles of conjugate gradient minimization). In the first minimization, a harmonic constraint was applied to all atoms of protein and ligand with a strength of 500 kcal/(mol·Å^2). It means that the water and counterions can move freely. This step is aimed to resolve the clashes between the solute and the solvent molecules. Then, a following minimization was performed without any constraint to eliminate possible remaining bad contacts in the system. After

minimization, the system was then heated from 0 to 300 K in 50 ps of simulation time at constant volume and equilibrated at a constant temperature of 300 K and a constant pressure of 1 atm for another 50 ps. The time step was set to 2 fs. The Particle-Mesh-Ewald (PME) method[53] was applied to calculate long-range electrostatics interactions. The SHAKE algorithm[54] was applied to constrain bonds involving hydrogen atoms. Periodic boundary conditions were applied to all dimensions.

2.4. MM-GB/SA Calculations. MM-GB/SA methodology was applied to calculate the binding free energies between the sEH and the inhibitors.[55−57] The first step of the method was to generate the snapshots from the MD trajectory. Before obtaining the snapshots, the water molecules and counterions in the MD trajectory should be stripped by the PTRAJ module of AMBER[48] since the solvent effect is described according to a GB/SA implicit solvent model. Then, 1000 snapshots of the ligand, receptor, and the corresponding complex were extracted from the last 20 ns of MD trajectory of the ligand−protein complex. For each snapshot, the binding free energy (ΔG_{bind}) of the inhibitor to the protein was calculated by the MM-GB/SA method as in the follow equation:

$$\Delta G_{bind} = G_{complex} - (G_{receptor} + G_{ligand}) \quad (1)$$

The binding free energy is estimated as a sum of the three terms:

$$\Delta\Delta G_{TOT} = \Delta G_{MM} + \Delta G_{sol} - T\Delta S \quad (2)$$

where ΔG_{MM} is the molecular mechanics component in gas phase, ΔG_{sol} is the solvation free energy, $T\Delta S$ is the change of conformational entropy on ligand binding. The molecular mechanics free energy (ΔG_{MM}) is further split into a van der Waals (ΔG_{vdw}) and electrostatic (ΔG_{ele}) energy:

$$\Delta G_{MM} = \Delta G_{ele} + \Delta G_{vdw} \quad (3)$$

The solvation free energy ΔG_{sol} can be divided into a electrostatic solvation free energy (ΔG_{GB}) and a nonpolar solvation free energy (ΔG_{SA})

$$\Delta G_{sol} = \Delta G_{GB} + \Delta G_{SA} \quad (4)$$

The ΔG_{GB} to the solvation energy is computed with a GB module (Onufriev's GB,[58] IGB = 2) of the AMBER suite.[48] In our calculations, the dielectric constant was set to 1.0 for the interior solute and 80.0 for the exterior solvent. The ΔG_{SA} was determined according to the eq 5:

$$G_{SA} = \gamma \times SASA + \beta \quad (5)$$

where γ is the surface tension proportionality constant and was set to 0.0072 kcal/(mol·Å^{-2}), and β is the offset value, which was 0 here. SASA, determined with the linear combination of pairwise overlaps (LCPO) model,[59] is the solvent accessible surface area and is estimated by the MSMS algorithm with a probe radius of 1.4 Å.

The entropy term ($-T\Delta S$) was computed through a normal-mode analysis (NMA) with the NMODE module in the AMBER10 program.[57] The computation was based on 50 snapshots taken from the final 20 ns of the MD trajectory with an even interval of 400 ps. Since the entropy term calculation is extremely time-consuming and has fairly high memory requirements for large systems, to reduce computational time and memory requirements, the eigenvectors for normal-mode analysis were not considered in this study.

3. RESULTS AND DISCUSSION

3.1. Molecular Dynamics Simulation. The first part of our research aims to determine the most possible protonation state of His523 located in the active site of the complex. For this purpose, we assigned to three different protonation states of histidine side-chain nitrogen atoms: histidine with hydrogen on the δ-nitrogen named Hid, on the ε-nitrogen named Hie, and on both nitrogen atoms named Hip. Other ionizable residues were set at their default protonation states at a neutral pH by the LEAP module.[48] The three systems were labeled as sEH/Hid523, sEH/Hie523, and sEH/Hip523, respectively. Six nanosecond molecular dynamics productions of different protonated complexes were performed as described in section 2. For each system, the crystal structure was used as the initial structure for MD. In order to assess the quality of the MD simulations, the rmsds of Cα atoms relative to the crystal structure were monitored along the entire MD trajectory of each complex by the PTRAJ model of the AMBER10 suit.[48] Figure 2 plots the rmsd values of the three systems as a function

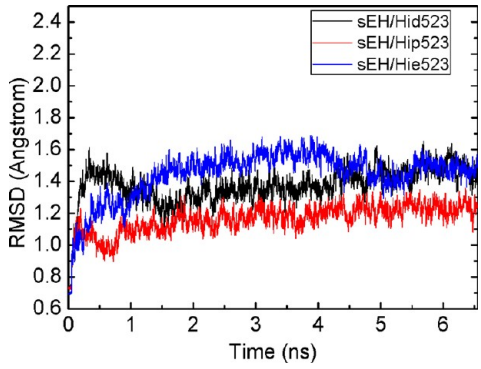

Figure 2. The rmsds of Cα atoms for the complex relative crystal structure.

of simulation time. One can see that, in the last 2 ns, the rmsd values are in equilibrium, which indicates that the trajectories of the three systems are stable. Subsequently, a total of 100 snapshots at a time interval of 20 ps from the final 2 ns of MD trajectories of the three systems were taken to calculate the binding free energy with MM-GB/SA method. On the basis of MM-GB/SA calculation, the average binding free energies of 100 conformations from the three systems are sEH/Hid523 (−41.54 ± 2.41 kJ/mol), sEH/Hie523 (−46.48 ± 2.00 kJ/mol), and sEH/Hip523 (−43.25 ± 2.30 kJ/mol), respectively. In the consideration of binding free energy, sEH/Hie523 has the lowest binding free energy of the lead compound to protein and it may be a favorable protonation state.

For comparison, the three average conformations of the last 2 ns of the MD simulation trajectories were superimposed on the crystal structure, respectively (see Figure 3). Figure 3 shows that the structures of key residues and lead compound of sEH/Hie523 system generally agree with those of the crystal structure, while both sEH/Hid523 and sEH/Hip523 are obviously different. On the basis of the above analysis, it can be concluded that the protonation state of Hie523 should be the most favorable protonation state. Because all of inhibitors in this study have the same functional group (benzoxazole) in the smaller hydrophobic pocket, the protonation state of His523 was set to be Hie523 and the other ionizable residues to be their default protonation states at a neutral pH for all systems in this study.

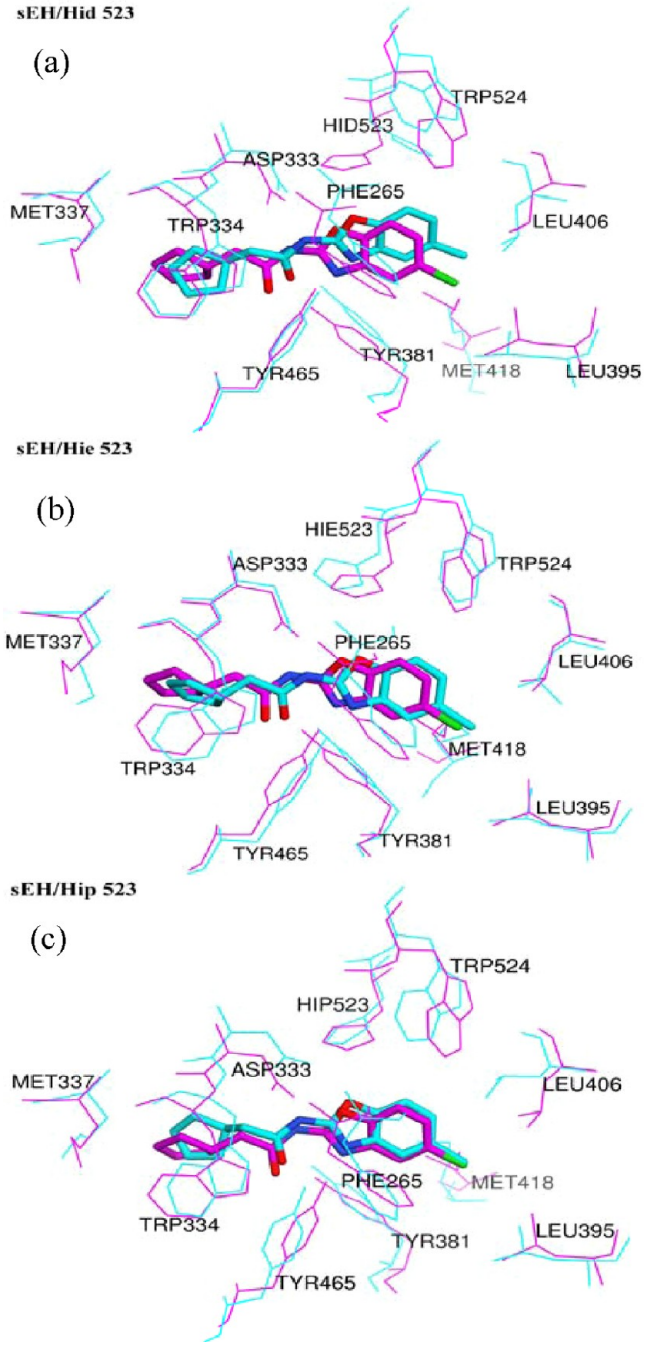

Figure 3. Three average conformations of different protonation states from the last 2 ns of MD trajectories were superimposed with the crystal structure via backbone atoms, respectively. In the superimpositions, the protein residues are shown in wire and the lead compound in stick. The crystal structures are colored in magenta and average structures in cyan. The figure is created by using Chimera software.[46]

Li et al.[30] speculated that a possible source of the 4-methylbenzoxazole and the 6-methybenzoxazole with poor potency against sEH is because the hydrogen bonds of Tyr381 and Tyr465 to the benzoxazole oxygen are much weaker than to the benzoxazole nitrogen when the benzoxazole ring of these two inhibitors undergoes a 180° rotation along the 2-benzoxazole bond, according to their docking results and the assumption that the benzoxazole ring remains at the orientation shown in the crystal structure. With the purpose of verifying the conjecture by Li et al.,[30] we flipped the benzoxazole ring 180° along the 2-benzoxazole bond and fixed the coordinates of the other moiety of these compounds from the docking structures. After this process, we got 12 conformations of six inhibitors, and then, they were classified into two groups (group A and group B) according to the orientation of the benzoxazole ring (shown in Table 1). To explore the stability, dynamics characteristics, and binding mode of the sEH complex with these ligands, the crystal structure, docking conformations, and modified conformations were used as the initial structures for MD simulations.

In order to sample enough conformations for calculating binding free energy, each system would stabilize in the equilibrium stage not less than 20 ns of simulation time. Following MD simulations, the stability of MD trajectory and the interactions including binding free energy, types of interaction, hydrogen bonds, and binding model predictions were analyzed and discussed below.

To monitor the dynamic stability during production phase, rmsd values of backbone atoms compared to the starting structure were calculated along the entire MD trajectory for each system. Owing to the fact that the flexibility of terminal loop residues would affect the actual rmsd values, only the residues (N231−A545) were taken into account. Figure 4 shows the time dependence of rmsds of sEH complexes with the seven ligands. The average and standard deviation of rmsd in the last 20 ns were sEH(1.57 ± 0.29 Å), sEH/lead compound(1.3 ± 0.24 Å), sEH/1a(1.63 ± 0.30 Å), sEH/1api(1.26 ± 0.25 Å), sEH/1b(1.36 ± 0.24 Å), sEH/1bpi(1.40 ± 0.23 Å), sEH/1c(1.24 ± 0.21 Å), sEH/1cpi(1.70 ± 0.26 Å), sEH/1d(1.37 ± 0.22 Å), sEH/1dpi(1.52 ± 0.35 Å), sEH/1e(1.51 ± 0.24 Å), sEH/1epi (1.38 ± 0.27 Å), sEH/1f(1.37 ± 0.27 Å), and sEH/1fpi (1.45 ± 0.28 Å), respectively. These values indicate distinctly that sEH does not exhibit substantial conformational changes. The rmsd curves in Figure 4 show that each system has attained equilibrium in the last 20 ns. Additionally, comparing the free sEH simulation to those bound simulations, it can be found that the rmsd values are higher than those of complexes, except the 1cpi simulation. This may imply that there are some slight conformational changes in the active site of the free sEH simulation because of the lack of hydrogen-bonding to stabilize key residues Asp333, Tyr381, and Tyr465. It is interesting that the curves of sEH/1b and sEH/1bpi overlap each other, suggesting that the two systems have similar dynamic behaviors. As for the sEH/1a, sEH/1cpi, sEH/1dpi, sEH/1f, and sEH/1fpi systems, a continual increase is observed in the previous period and flattens out after that, while sEH/1api, sEH/1c, sEH/1d, and sEH/1epi systems tend to converge at the early stage of simulations. The rmsd profile of sEH/1e system keeps ∼1.2 Å during the first 20 ns and ∼1.5 Å during the last 20 ns. This suggests that there are some conformational changes between the two periods. As a whole, all systems approach accepted equilibrium states during the last 20 ns.

3.2. Binding Free Energy Calculation. According to the rmsd analysis, MM-GB/SA calculation and subsequent free energy decomposition in each case were based on the last 20 ns of MD trajectory at an interval of 20 ps. All of the energy terms and the entropy changes were listed in Table 2. For each compound with two binding modes, the one that has the lower $\Delta\Delta G_{TOT}$ is believed to be a more favorable binding mode. According to the calculated results of $\Delta\Delta G_{TOT}$, the more likely binding mode for each compound is selected, they are sEH/

dx.doi.org/10.1021/jp304736e | J. Phys. Chem. B 2012, 116, 10219−10233

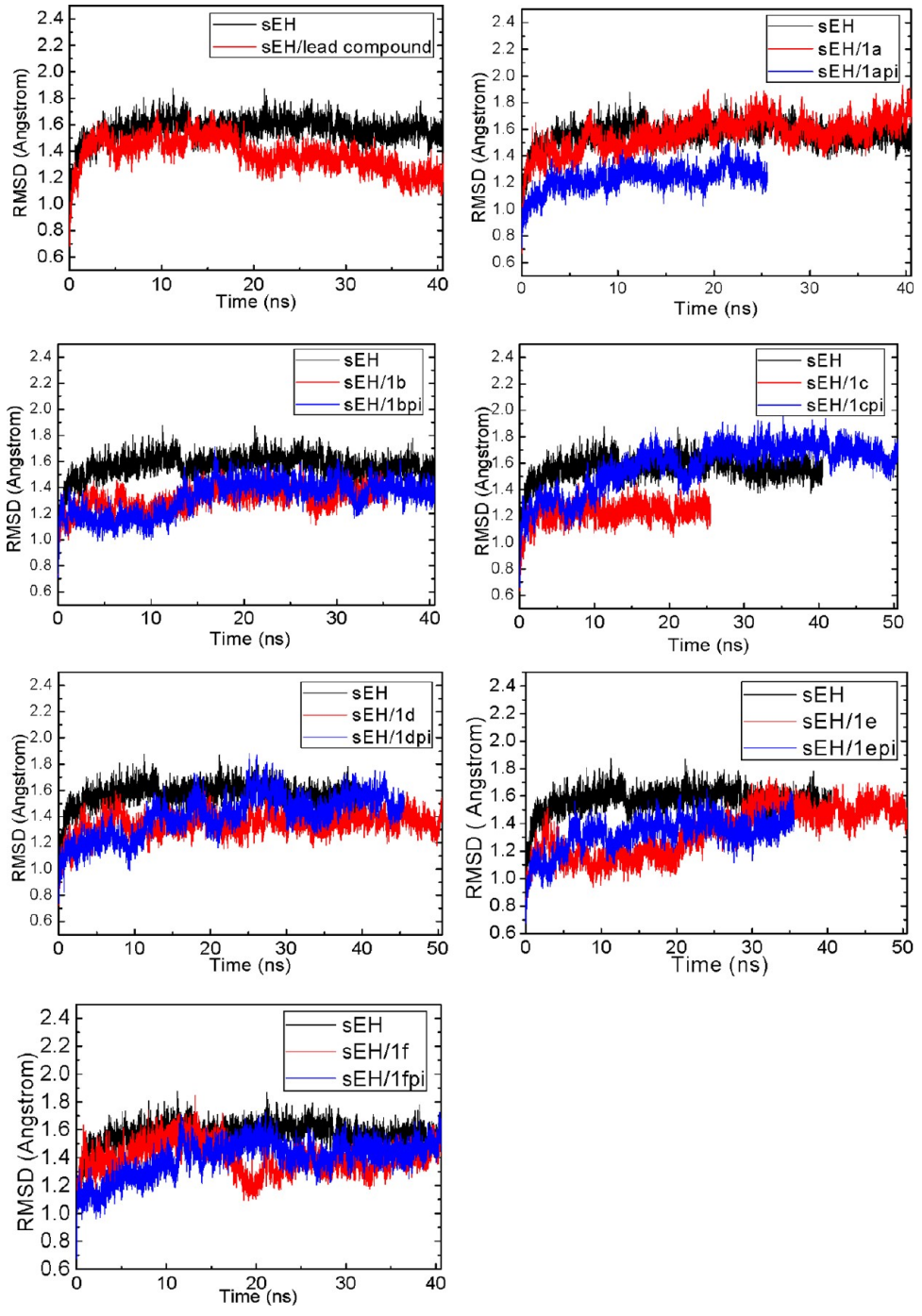

Figure 4. Rmsds of backbone atoms of unliganded protein and all complexes relative to the initial structure.

1api, sEH/1b, sEH/1c, sEH/1d, sEH/1epi, and sEH/1fpi, respectively. In the sight of these binding modes, the predication of $\Delta G_{\text{MM-GB/SA}}$ can give a reasonable ranking of binding strength. When the entropy term is taken into account by using NMA, the overall ranking of $\Delta\Delta G_{\text{TOT}}$ of this set of compounds is in complete accord with that of experimental IC_{50} values. It is worth noting that there is an approximately linear relationship (correlation coefficient, $r^2 = 0.88$) between the predicted binding free energy ($\Delta\Delta G_{\text{TOT}}$) and experimental bioactivity data (IC_{50}), indicating the parameters applied to calculate the free energy are feasible and reliable.

It can be seen from Table 2 that the van der Walls (ΔE_{vdw}), electrostatic (ΔE_{elec}) and nonpolar solvation terms (ΔG_{SA}) are favorable for ligand binding to sEH protein while the polar solvation and entropy terms are unfavorable for binding in all the 13 complexes. Besides, the van der Waals energies contribute the most component of the binding free energy for each complex (from −41 to −57 kcal/mol). This indicates that the van der Waals interactions are crucial in stabilizing the sEH−ligand complex, and shape complementarity is the primary factor that dominates the affinities of these inhibitors binding upon sEH. However, the ΔG_{elec} term is always a positive number (unfavorable) for all complexes in this study. It is because the gas-phase electrostatic interactions reformed (ΔE_{elec}) between the protein and the ligand cannot fully compensate the unfavorable effect generated by electrostatic

dx.doi.org/10.1021/jp304736e | J. Phys. Chem. B 2012, 116, 10219−10233

Table 2. Binding Free Energies (kcal/mol) of Each sEH/Inhibitor Complex Calculated by MM-GB/SA Method and NMA

system	ΔE_{elec}	ΔE_{vdw}	ΔG_{SA}[a]	ΔG_{GB}	ΔG_{elec}[b]	$\Delta G_{MM\text{-}GB/SA}$[c]	$-T\Delta S$	$\Delta\Delta G_{TOT}$[d]	IC_{50} (nM)[e]
3PDC	−28.72	−41.24	−4.94	30.02	1.30	−44.88	13.30	−31.58	32
sEH/1a	−36.71	−46.76	−6.61	46.08	9.37	−44.01	22.51	−21.50	
sEH/1api	−36.04	−49.88	−6.83	44.99	8.95	−47.76	20.76	−27.00	94.3
sEH/1b	−35.29	−54.93	−6.97	41.62	6.33	−55.57	18.90	−36.67	6.92
sEH/1bpi	−36.16	−52.91	−7.03	44.17	8.01	−51.94	21.12	−30.82	
sEH/1c	−33.66	−56.70	−6.87	41.91	8.25	−55.32	22.54	−32.78	11.4
sEH/1cpi	−30.45	−52.77	−7.17	41.56	11.11	−48.83	24.46	−24.37	
sEH/1d	−32.52	−52.73	−7.35	42.67	10.15	−49.93	20.41	−29.52	73
sEH/1dpi	−27.91	−55.79	−7.38	39.14	11.23	−51.93	24.15	−27.78	
sEH/1e	−23.15	−57.21	−7.25	34.36	11.21	−53.25	32.64	−20.61	
sEH/1epi	−21.70	−49.42	−6.90	32.62	10.92	−45.40	23.32	−22.08	272
sEH/1f	−31.46	−53.08	−6.76	40.89	9.43	−50.42	29.44	−20.98	
sEH/1fpi	−34.63	−52.46	−7.00	44.80	10.17	−49.29	26.21	−23.08	202

[a] $\Delta G_{SA} = \gamma \times SASA + \beta$; $\gamma = 0.0072$ kcal/(mol·Å^{-2}); $\beta = 0$. [b] $\Delta G_{elec} = \Delta E_{elec} + \Delta G_{GB}$. [c] $\Delta G_{MM\text{-}GB/SA} = \Delta E_{elec} + \Delta E_{vdw} + \Delta G_{SA} + \Delta G_{GB}$. [d] $\Delta\Delta G_{TOT} = \Delta E_{elec} + \Delta E_{vdw} + \Delta G_{SA} + \Delta G_{GB} - T\Delta S$. [e] IC_{50} was taken from an experiment measured by Li et al.[30]

interactions between solute molecules (the protein and the ligand) and solvent molecules. In other words, the electrostatic interactions between ligand and receptor are weaker than that between ligand and solvent. This clearly reflects that electrostatic interactions are unfavorable for ligand binding, when a ligand moves from solvent environment to the active site of protein. Moreover, both ΔE_{vdw} and ΔG_{SA} of the six compounds relative to the lead compound are improved. This is because the ΔE_{vdw} and ΔG_{SA} correlate with the size of the molecule. It is worth noting that the entropy term ($-T\Delta S$) has a comparable magnitude to the electrostatic interactions. Hence, it also plays an important role in determining the binding free energy of the ligand binding to the macromolecular target. The entropy term, due to the loss of degrees of freedom upon association, is decomposed into translational, rotational, and vibrational contributions. Our results show that the loss of entropy for all 12 complexes is higher than the crystal structure bound lead compound. One possible reason is when the cyclopentyl moiety of the lead compound was substituted by 1-piperidinecarboxylic acid, 1,1-dimethylethyl ester, the six inhibitors became more flexible and lost more conformational entropy during binding upon sEH protein reduced their degrees of freedom. The other reason may be that the conformational rearrangement during inhibitors upon sEH binding is accompanied by a significant loss of entropy. In addition, if the binding free energy without including the contribution of entropy only originates from the contribution of enthalpy ($\Delta G_{MM\text{-}GB/SA}$), 1e and 1f binding modes seems to be more favorable than corresponding 1epi and 1fpi binding modes. It can be seen that the entropy may improve the correlations between the ranking of predicted binding free energy ($\Delta\Delta G_{TOT}$) and that of experimental inhibitory activity (IC_{50}). On the basis of the above analysis, it can be suggested that the entropy term plays an indispensable role in predicting binding free energy for these complexes.

3.3. Binding Modes of sEH/Inhibitors Complex and Hydrogen Bond Analysis. For better visualizing and comparing the binding mode of each complex, the average structures of the sEH/lead compound, sEH/1api, sEH/1b, sEH/1c, sEH/1d, sEH/1epi, and sEH/1fpi from the last 20 ns of each MD trajectory, were overlapped (Figure 5). As shown in Figure 5, the benzoxazole moiety of the six compounds occupied almost the same binding pocket as that of the lead compound; however, compared with benzoxazole moiety of

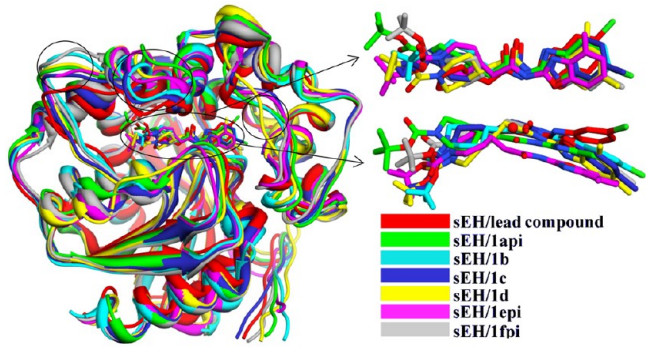

Figure 5. Superposition of the average structure of sEH/lead compound, sEH/1api, sEH/1b, sEH/1c, sEH/1d, sEH/1epi, and sEH/1fpi from the last 20 ns molecular simulation trajectories. The inhibitors are shown in stick representation and the oxygen atom of the amide of the lead compound is represented as a ball independently. The figure is created by using Chimera software.[46]

lead compound, benzoxazole moieties of them slightly rotate toward the entrance of the smaller lipophilic pocket around the connecting bond to amide. It can be seen from the amide moiety of the inhibitors in Figure 5 that six inhibitors comparing with lead compound undergo little movements toward the smaller lipophilic pocket. One possible reason is that substitution of the cyclopentyl group with 1-piperidinecarboxylic acid, 1,1-dimethylethyl ester enlarges the size of the inhibitors, which results in a closer contact with residues in the larger hydrophobic pocket. In order to avoid steric clash, the inhibitors are pushed toward the smaller pocket. Because of the flexibility of inhibitor and adequate interspaces between residues and ligand in the larger pocket, the conformations of 1-piperidinecarboxylic acid, 1,1-dimethylethyl ester moiety of these inhibitors have obvious differences. In addition, from the superposed conformation, the binding pocket shape for each complex has no substantial deviation. This may be partly accounted for those compounds with the same structure except different substituent groups at benzoxazole moiety. However, one can find that three domains were shifted slightly, a turn (K374-D380) between two α helix and two loops (P359-S368 and A409-K420), which were marked by black circles in Figure 5. The reason may lie in the fact that the regions being fully exposed to the water solvent weaken the interaction with surround residues and have therefore high flexibility.

dx.doi.org/10.1021/jp304736e | J. Phys. Chem. B 2012, 116, 10219−10233

For reducing the size of this study, five representative complexes (sEH/lead compound, sEH/1b, sEH/1bpi, sEH/1e, and sEH/1epi) were chosen and analyzed here. Figure 6 shows

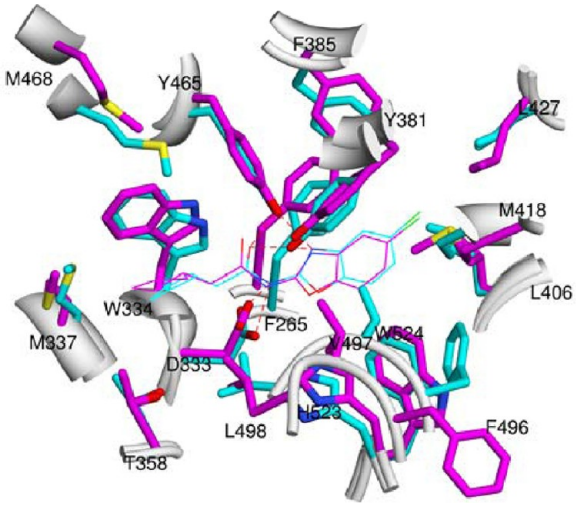

Figure 6. Crystal structure superimposed with the average structure form the last 20 ns MD trajectory of this complex. The inhibitors are shown in wire representation. The residues are shown in stick. The crystal structure and average structure are colored with magenta and cyan, respectively. Hydrogen bonds are shown in red dash lines. The figure is created by using Chimera software.[46]

the superimposition of the crystal structure with the average structure from the last 20 ns MD simulation of this complex. Partial amino acid residues interacting with ligand in the binding site have been displayed. In the first place, the ligand and key residues possess almost the same conformation, which suggest that the simulated structure generally reproduces the experimental determined one, and the lead compound extends deeply into two hydrophobic pockets in the sEH active site. The 5-chlorobenzoxazole moiety locates in the smaller pocket, formed by several hydrophobic amino acids (Phe265, Pro266, Phe385, Leu395, Leu406, Leu416, Met418, Leu427, Phe496, Val497, and Trp524). Benzene ring of Phe265 side chain could form T-shaped aromatic interaction with 5-chlorobenzoxazole moiety of the inhibitor. The phenyl ring of Phe496 that situates on a loop region undergoes a large movement relative to the residue in the crystal structure. The amide moiety of the lead compound is stabilized and oriented by three catalytic residues (Asp333, Tyr381, and Tyr465) via six hydrogen bonds. The carbonyl oxygen atom (O19) of amide forms two hydrogen bonds with the hydroxyl groups of Tyr381 (−O19···HO) and Tyr465 (−O19···HO), respectively. The amide nitrogen (N11) could form two hydrogen bonds with two oxygen atoms of the catalytic aspartate residue Asp333. The hydroxyl groups of Tyr381 and Tyr465 could also form two hydrogen bonds with the nitrogen atom (N1) of the benzoxazole moiety (OH···N1−). Moreover, the cyclopentyl group, which interacts with hydrophobic residues (Met337, Met468, Val497, and Leu498), occupies the larger pocket and forms a stacking interaction with the indole side chain of residue Trp334.

For the ease of comparison, the average structures of sEH/lead compound and sEH/1b during the final 20 ns MD trajectories are overlapped. The geometries of major residues, which afford main interactions with inhibitors, are plotted in Figure 7. Those residues in the smaller pocket are shown in

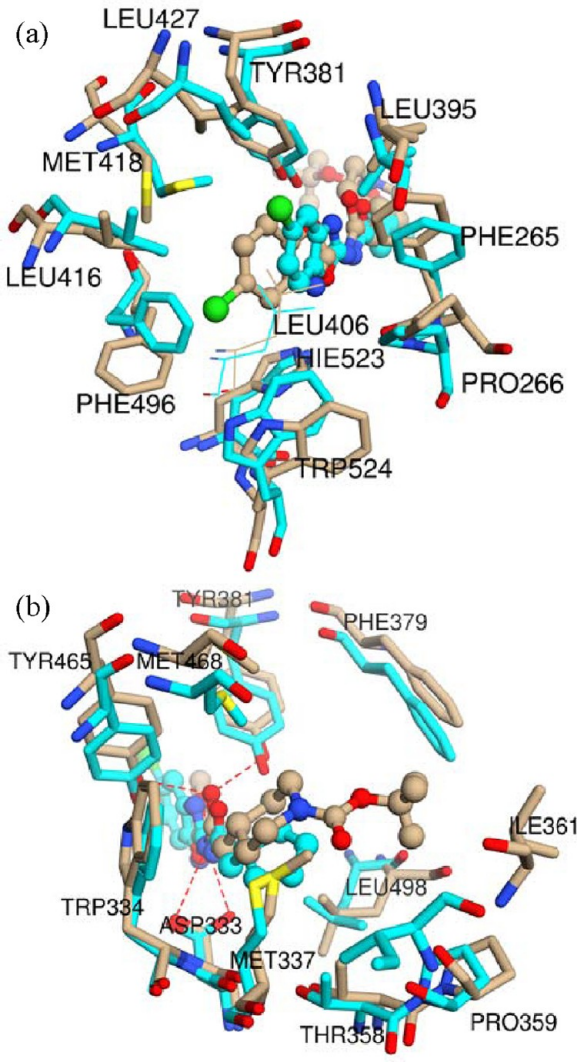

Figure 7. Superposition of the average structure of sEH/lead compound and the average structure of sEH/1b from the last 20 ns MD trajectories. sEH/lead compound was colored with cyan and sEH/1b with tan. The inhibitors were represented with ball and stick and residues with stick. Hydrogen bonds are shown in red dash lines. (a) Viewed from the smaller pocket; (b) viewed from the larger pocket. The figure is created by using Chimera software.[46]

Figure 7a, and those in the larger pocket are shown in Figure 7b. To avoid steric clash with Leu406, 5-chlorobenzoxazole moiety of compound 1b takes a slight deviation relative to the lead compound (shown in Figure 7a). It also undergoes a 180° rotation along the 2-benzoxazole bond, resulting in the chlorine atom pointing to residue Phe496 and forming a closer van der Waals contact with Phe496. We also find that the benzoxazole moiety of the 1b binding mode leads to local structural changes. The side chains of Phe496 and Trp524 obviously deviate from the corresponding residues in the average structure of the sEH/lead compound complex, but the T-shaped aromatic interaction between the benzene ring of Phe265 side chain and 5-chlorobenzoxazole moiety of sEH/1b is maintained well. Figure 7b presents the contact status of 1-piperidinecarboxylic acid, 1,1-dimethylethyl ester moiety of compound 1b and cyclopentyl of the lead compound with those residues in the larger pocket. As shown in Figure 7b, when the lead compound is replaced by compound 1b, the larger lipophilic pocket adjusts

dx.doi.org/10.1021/jp304736e | J. Phys. Chem. B 2012, 116, 10219−10233

its conformation to accommodate formic acid, 1,1-dimethylethyl ester moiety of 1b, especially, Ile361 taking a significant movement. Because of a larger molecular size, the ester moiety produces a closer van der Waals contact with Pro359, Ile361, and Phe379 than the cyclopentyl group. In the sEH/1b complex, the piperidine ring in place of the cyclopentyl group forms a stacking interaction with the indole side chain of Trp334. Compared with the lead compound, the whole molecule 1b takes a translation motion from the larger pocket to the smaller pocket, and thus, the distances between the oxygen atom (O3) of benzoxazole and the hydroxyl of Tyr381 and Tyr465 are increased. Because of the long distance (3.49 Å) between the O3 of benzoxazole and the hydroxyl of Tyr465, they could not form stable H-bond. By comparison with the sEH/1b complex, just a little conformational change of residues in the smaller pocket of the sEH/1bpi complex has been found (shown in Figure 8). It may be the reason that sEH/1b and sEH/1bpi have similar dynamic behaviors. In addition, sEH/1c and sEH/1fpi systems have the same binding mechanisms as sEH/1b does.

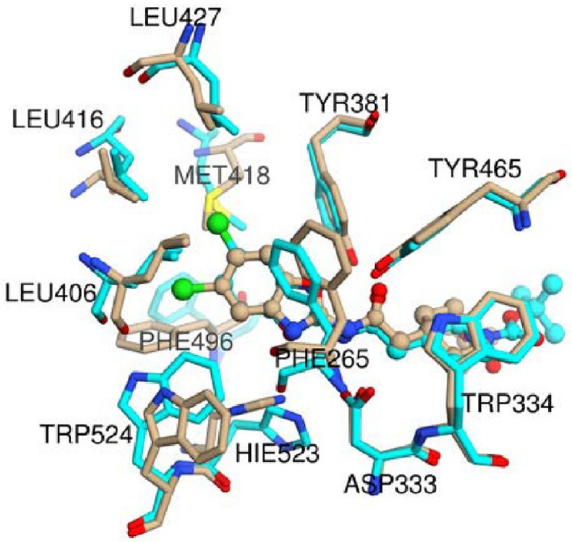

Figure 8. Overlapped conformation of binding pocket of the average structure of sEH/1b and sEH/1bpi from the last 20 ns MD simulations. The inhibitors were represented with ball and stick and residues with stick. sEH/1b was colored with tan and sEH/1bpi colored with cyan. The figure is created by using Chimera software.[46]

Figure 9 provides a visual inspection of the superposition of the averaged structure of sEH/1e and sEH/1epi from the last 20 ns MD trajectories. From Figure 9, it can be seen that 4-methyl of 1e binding mode points to residue Hie523. For alleviating steric clash with Hie523, 4-methylbenzoxazole moiety is repulsed toward a cleft between Tyr381 and Gln385. It is most probably because of residue Hie523 forming several strong H-bonding interactions with other residues. Thus, it is restrained in a fixed place. This can be confirmed by the rmsd values of residue Hie523 around 0.05 Å during MD simulation (the figure was not shown). In the case of the 1epi binding mode, the conformational changes in the binding pocket take place as a methyl substituted at the 4 position of benzoxazole. In particular, the side chains of Tyr381 and Tyr465 deviate from the corresponding residues in the original crystal structure. Furthermore, the N1 atom of benzoxazole in compound 1epi and the hydroxyl groups of Tyr381 and Tyr465

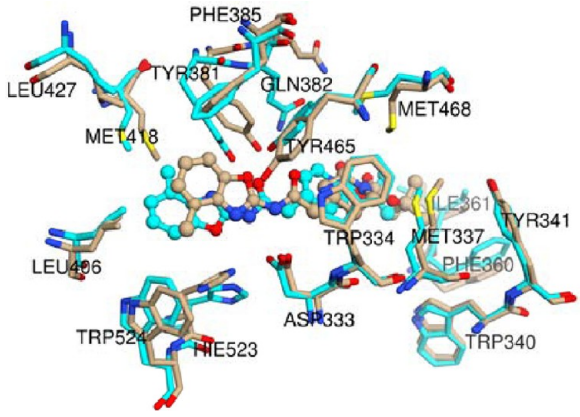

Figure 9. Overlapped conformation of binding pocket of the average structure of sEH/1e and sEH/1epi from the last 20 ns MD simulation. The inhibitors were represented with ball and stick and residues with stick. sEH/1e was colored with tan and sEH/1epi with cyan. The figure is created by using Chimera software.[46]

no longer form a stable hydrogen bonding interaction because of the long distances (3.45 Å and 4.61 Å) between them. Besides, we also calculated the B-factors of these two complexes, which have often been used as indicating the mobility and flexibility of different parts of the structure. It can be calculated by using the formula $B = 8\pi^2/3\langle\Delta r^2\rangle$, where $\langle\Delta r^2\rangle$ is the mean-square atomic positional fluctuations (RMSF). Figure 10 represents the B-factors for the backbone

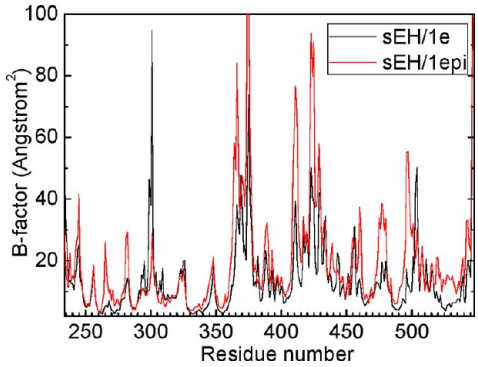

Figure 10. B-factors of the backbone atoms (Cα, N, and C) versus residue number for sEH/1e and sEH/1epi complexes.

of these two complexes. Interestingly, the B-factors of backbone atoms in sEH/1epi are generally higher than the ones in sEH/1e, indicating that the flexibility of protein increases in the sEH/1epi binding mode. From this finding, we can draw a conclusion that the loss of degrees of freedom favoring binding in the sEH/1e system is larger than in the sEH/1epi system. Therefore, 1e binding mode loses more entropy than 1epi binding mode. This result is in agreement with that provided by NMA. This means that the contribution of entropy should not be ignored for these complexes. In the case of 5,7-dimethylbenzoxazoles, in order to avoid steric clash with residue Hie523, 7-methyl has an analogical orientation as 4-methyl of the sEH/1epi complex does. Simultaneously, the orientation of 5-methyl is equivalent to that of the 5-chloro of the 1b binding mode. 5-Methyl of sEH/1d, getting a closer van der Waals contact with Leu406, promotes ligand association.

In order to further investigate the influence of the configuration on the hydrogen bonding network, hydrogen

dx.doi.org/10.1021/jp304736e | J. Phys. Chem. B 2012, 116, 10219−10233

Table 3. Percentage of Hydrogen Bonds during MD Simulations between the Inhibitor and the Residues around the Inhibitor[a]

inhibitor	donor	acceptor	occupancy (%)	distance (Å)	angle (deg)
lead compound	Asp333@OD2	inhibitor@N11−H4	99.85	2.807(0.10)	16.05(9.29)
	inhibitor@N1	Try465@OH−HH	93.83	3.014(0.16)	31.77(13.94)
	inhibitor@O19	Try381@OH−HH	93.70	2.958(0.20)	27.99(12.37)
	inhibitor@O19	Try465@OH−HH	58.31	3.097(0.22)	41.17(11.46)
	inhibitor@N1	Try381@OH−HH	51.18	3.191(0.17)	45.76(10.27)
	Asp333@OD1	inhibitor@N11−H4	49.85	3.222(0.18)	46.70(9.66)
1a	Asp333@OD1	inhibitor@N11−H4	96.43	2.980(0.18)	28.25(13.68)
	inhibitor@O19	Try381@OH−HH	94.44	2.966(0.20)	27.41(12.79)
	inhibitor@O19	Try465@OH−HH	92.41	3.003(0.21)	25.20(11.58)
	Asp333@OD2	inhibitor@N11−H4	90.81	2.884(0.15)	35.66(13.78)
	inhibitor@O3	Try381@OH−HH	68.14	3.091(0.20)	45.15(10.45)
	inhibitor@O3	Try465@OH−HH	54.08	3.144(0.20)	47.89(8.67)
1api	Asp333@OD2	inhibitor@N11−H4	97.93	2.810(0.11)	25.53(14.82)
	inhibitor@O19	Try381@OH−HH	96.01	2.919(0.19)	28.09(12.90)
	inhibitor@O19	Try465@OH−HH	91.28	2.993(0.21)	29.56(12.36)
	inhibitor@N1	Try381@OH−HH	55.49	3.191(0.18)	44.88(10.89)
	Asp333@OD1	inhibitor@N11−H4	50.96	3.115(0.21)	29.93(13.28)
	inhibitor@N1	Try465@OH-HH	46.45	3.236(0.17)	45.45(10.00)
1b	Asp333@OD2	inhibitor@N11−H4	99.74	2.807(0.10)	24.22(12.03)
	inhibitor@O19	Try381@OH−HH	99.67	2.830(0.16)	20.89(10.93)
	inhibitor@O19	Try465@OH−HH	98.71	2.796(0.14)	27.78(12.43)
	Asp333@OD1	inhibitor@N11−H4	89.81	3.108(0.18)	39.94(10.43)
	inhibitor@O3	Try381@OH−HH	44.94	3.194(0.18)	49.77(8.01)
1bpi	Asp333@OD2	inhibitor@N11−H4	99.83	2.776(0.09)	20.93(10.35)
	inhibitor@O19	Try381@OH−HH	96.38	2.931(0.19)	26.39(12.77)
	inhibitor@O19	Try465@OH−HH	92.06	2.952(0.21)	31.01(13.03)
	inhibitor@N1	Try381@OH−HH	55.55	3.153(0.18)	46.30(10.10)
	inhibitor@N1	Try465@OH−HH	49.01	3.213(0.18)	42.22(11.38)
1c	Asp333@OD2	inhibitor@N11−H4	99.84	2.828(0.11)	20.15(11.31)
	inhibitor@O19	Try465@OH-HH	98.48	2.829(0.17)	23.80(11.90)
	Asp333@OD1	inhibitor@N11−H4	69.05	3.186(0.18)	41.07(10.92)
	inhibitor@O24	Gln382@NE2−HE2	60.67	3.005(0.18)	31.60(13.10)
	inhibitor@N1	Hie523@NE2−HE2	49.58	3.195(0.15)	42.37(12.55)
1cpi	Asp333@OD1	inhibitor@N11−H4	80.02	2.980(0.22)	24.50(14.13)
	inhibitor@N1	Try465@OH−HH	73.79	3.129(0.18)	28.64(14.36)
	Asp333@OD2	inhibitor@N11−H4	72.11	3.024(0.24)	29.50(15.04)
1d	inhibitor@O19	Try465@OH−HH	99.00	2.851(0.16)	25.65(12.13)
	inhibitor@O19	Try381@OH−HH	98.33	2.882(0.18)	23.27(12.02)
	Asp333@OD2	inhibitor@N11−H4	96.58	2.945(0.16)	33.79(13.80)
	Asp333@OD1	inhibitor@N11−H4	91.94	2.989(0.19)	28.90(12.90)
	inhibitor@O3	Try381@OH−HH	50.46	3.193(0.17)	47.83(9.35)
1dpi	inhibitor@N1	Try465@OH−HH	98.93	2.979(0.15)	17.52(9.76)
	Asp333@OD2	inhibitor@N11−H4	96.16	2.974(0.18)	20.85(10.71)
	Asp333@OD1	inhibitor@N11−H4	81.22	3.091(0.20)	41.19(11.23)
1e	Asp333@OD2	inhibitor@N11−H4	96.57	2.987(0.17)	29.54(12.49)
	Asp333@OD1	inhibitor@N11−H4	93.21	3.036(0.19)	33.00(12.48)
	inhibitor@O3	Try465@OH−HH	81.31	3.125(0.19)	21.14(11.20)
1epi	Asp333@OD2	inhibitor@N11−H4	98.24	2.862(0.13)	23.14(12.20)
	inhibitor@O19	Try381@OH-HH	85.91	2.894(0.21)	26.95(13.44)
	inhibitor@N1	Try381@OH−HH	40.66	3.252(0.16)	44.27(11.23)
1f	Asp333@OD2	inhibitor@N11−H4	98.21	2.956(0.16)	25.92(12.04)
	inhibitor@O19	Try381@OH-HH	96.37	2.927(0.19)	21.20(11.03)
	inhibitor@O19	Try465@OH−HH	95.90	2.896(0.19)	28.75(12.90)
	Asp333@OD1	inhibitor@N11−H4	92.31	2.929(0.16)	38.82(11.91)
	inhibitor@O3	Try465@OH−HH	66.19	2.999(0.18)	47.07(9.71)
	inhibitor@N1	Hie523@NE2−HE2	57.87	3.074(0.15)	45.04(10.98)
	inhibitor@O3	Try381@OH−HH	47.08	3.204(0.18)	47.83(9.38)
1fpi	inhibitor@O19	Try465@OH−HH	95.22	2.931(0.20)	28.23(12.92)
	Asp333@OD1	inhibitor@N11−H4	94.73	2.992(0.19)	25.37(14.05)
	Asp333@OD2	inhibitor@N11−H4	86.58	2.890(0.15)	36.56(15.14)
	inhibitor@O21	Glu382@NE-HE2	46.71	3.192(0.18)	17.84(9.47)

Table 3. continued

[a]For every system, the cut-off used for hydrogen bond distance and angle was 3.5 Å and 120°, respectively. The percent hydrogen bond occupancy that hydrogen bonds formed during the MD simulations is produced by the PTRAJ module of AMBER 10.[48]

bond analyses were performed by the PTRAJ module of AMBER10[48] during the MD simulations, and the results were listed in Table 3. Hydrogen bonds were counted with the distance cutoff (3.5 Å between two heavy atoms) and angle cutoff (120° among heavy atom−hydrogen−heavy atom). As shown in Table 3, hydrogen bonds form mainly between three residues (Asp333, Tyr381, and Tyr465) and inhibitors. They play a crucial role in anchoring the inhibitors to the exact site and orientation for binding with sEH. In particular, a highly stable hydrogen bond between Asp333 and the N11 atom of the amide of the ligands exceeds 90% during all MD simulations. Moreover, Tyr465 could form a highly stable H-bond with N1 of 5-chlorobenzoxazole moiety (93.83%) in the sEH/lead compound, while the hydrogen bonding interaction between Tyr381 or Tyr465 and the O3 or N1 atom of other analogous compound obviously decreases. In line with previous Li's postulate,[30] if the benzoxazole ring of these designed inhibitors maintains the binding site and orientation as elucidated by the crystal structure, the hydrogen atom of the hydroxyl group of tyrosine residue bonding to the N1 atom is more stable than to the O3 atom. As shown in Figure 5, however, these six inhibitors in the binding pocket have a slight deviation, and hydrogen bonding interactions with the benzoxazole ring diminish relative to the lead compound. So, there is not much impact on whether benzoxazole flipped. It can also be verified by free energy decomposition in the next section that the differences of the contribution of binding free energies of Tyr381 and Tyr465 are negligible between the two binding modes of each complex. Therefore, the hydrogen bond that forms between two tyrosine residues and a nitrogen or oxygen atom is not the primary fact in determining the inhibitors active against sEH for the two binding modes of each complex.

3.4. Decomposition Analysis of the Binding Free Energy. In order to clearly discern the contributions of binding free energy of each residue, the interaction energies were further decomposed into individual residue contributions through the MM-PBSA script in the AMBER10 suite.[60] This quantitative information about decomposition is extremely useful in understanding the effects of different substitutions and binding modes. The decomposition of free energy on per-residue consists of molecular mechanics and solvation energy but does not include entropy changes.

As showed in Figure 11, these complexes have a similar interaction pattern, which indicates that all of them have the similar binding mode. Obviously, residue Trp334 serves as a crucial residue in all systems, contributing the most binding free energies, indicating that the aromatic interactions are critical for inhibitors binding to sEH. In addition, careful comparison of the two binding modes of each complex finds that the contributions of Tyr381 and Tyr465 to binding free energy are almost unaffected after benzoxazole is flipped. It must be pointed out that the contribution of Tyr465 of sEH/1epi, which is larger than the contribution of Tyr465 of sEH/le, is not caused by the hydrogen bond because it cannot form a hydrogen bond with ligand 1epi. In other words, the contributions of Tyr381 or Tyr465 will not be influenced, regardless of whether the residue forms an H-bonding interaction with oxygen atom or nitrogen atom. This is not consistent with Li's results of conjecture,[30] which believes that the 4-methylbenzoxazole and the 6-methybenzoxazole with poor potency against sEH are because the hydrogen bonds of Tyr381 and Tyr465 to the benzoxazole oxygen are much weaker than to the benzoxazole nitrogen. One possible reason is that hydrogen bonding occupancies of Tyr381 and Tyr465 in these systems are lower than the corresponding ones in the sEH/lead compound complex.

Finally, we discuss the reasons why these six amide inhibitors have variant inhibitory potency. Since these compounds have the same structure in the larger pocket, we can surmise that different inhibitory potency may derive from the van der Waals interactions of the smaller hydrophobic pocket. If we define the larger pocket composed by the residues Trp334, Met337, Trp340, Tyr341, Thr358, Pro359, Phe360, Ile361, Pro369, Phe379, Met468, and Leu498 and the smaller pocket by the residues Phe265, Pro266, Phe385, Ser405, Leu406, Leu416, Met418, Leu427, Phe496, and Val497, the binding affinities of two hydrophobic pockets in the six complexes are listed in Table 4. It can be seen from Table 4 when the cyclopentyl group of the lead compound was substituted, the van der Waals interactions between ligand and residues in the larger pocket increase. Although six designed inhibitors have different conformations, their contributions to binding free energy are nearly identical. Furthermore, if we arrange the contributions of binding free energy of the smaller pocket in descending sequence, we will find that the order (sEH/1b, sEH/1c, sEH/1, sEH/1d, sEH/1a, sEH/1fpi, and sEH/1epi) is consistent with that of experimental IC_{50} values, indicating that the binding strengths of inhibitors depend on orientations of benzoxazole and substitution positions. It is because the benzoxazole pocket of the sEH binding site is relatively enclosed and different substituted positions directly influence the interactions between ligand and receptor. In order to get a better view, the contribution of key residues of seven complexes was compared and plotted in Figure 12. Here, we nominate those residues that contribute binding free energies lower than −1.0 kcal/mol as key residues. It is notable that the Asp333, Tyr381, and Tyr465 in sEH/lead compound complex contribute more binding free energies than in the other systems. This is because these inhibitors undergo a slight movement relative to the site of the lead compound revealed in crystal structure. So the distances between the inhibitor and the three residues are changed in these systems and the interactions between them are influenced.

In summary, the variant potency of these designed inhibitors mainly derives from the van der Waals interaction. The potency of these compounds to the sEH protein is not decided by hydrogen bonds or a certain residue but by the common effect of multiple residues in binding pocket.

4. CONCLUSIONS

The binding modes and interaction mechanisms of soluble epoxide hydrolase with a class of amide inhibitors, which based on Li's experiments,[30] were explored by using molecular docking and dynamic simulation. MM-GB/SA binding free energy calculation of the protein−ligand complex was

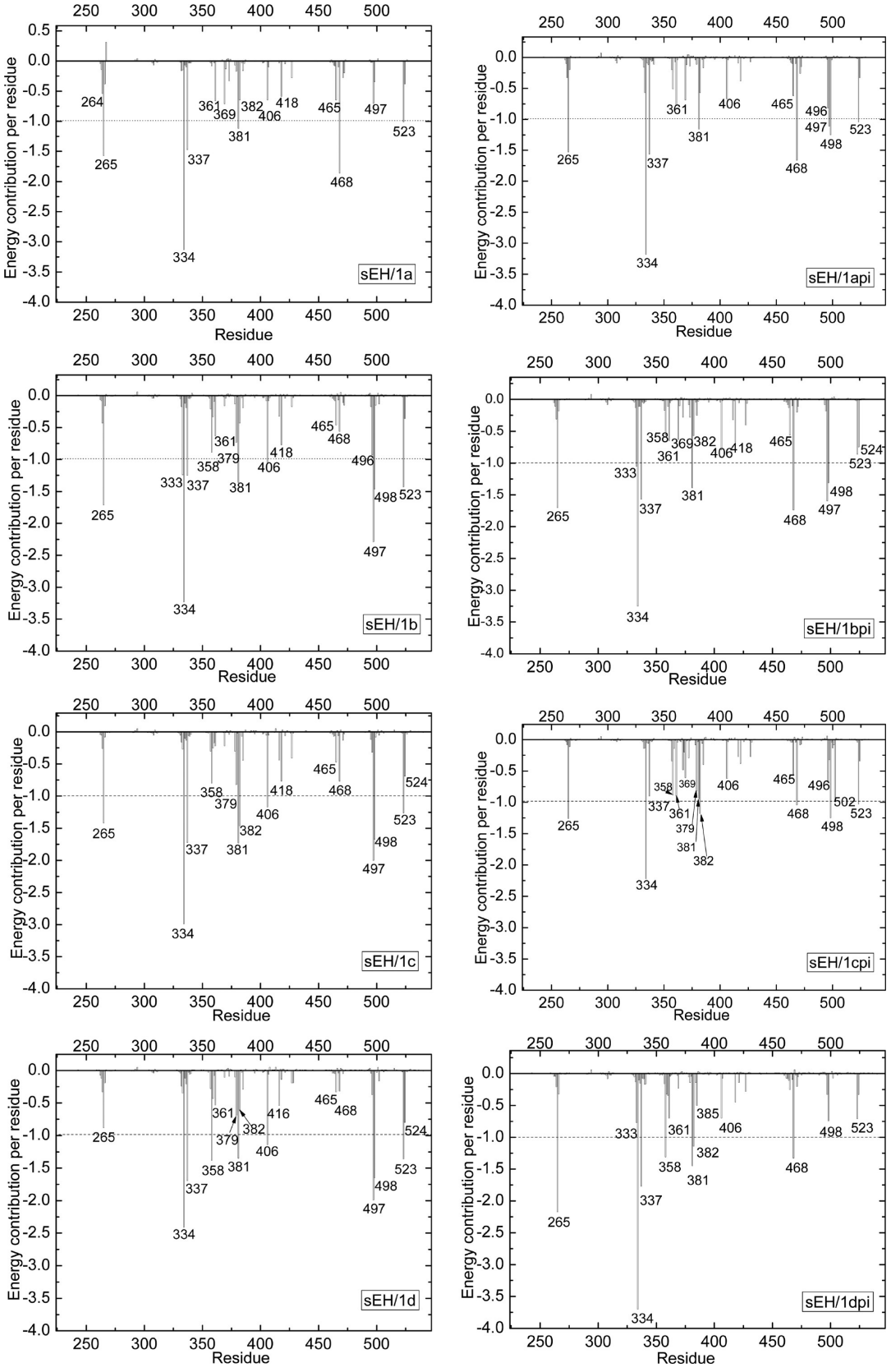

Figure 11. continued

dx.doi.org/10.1021/jp304736e | J. Phys. Chem. B 2012, 116, 10219−10233

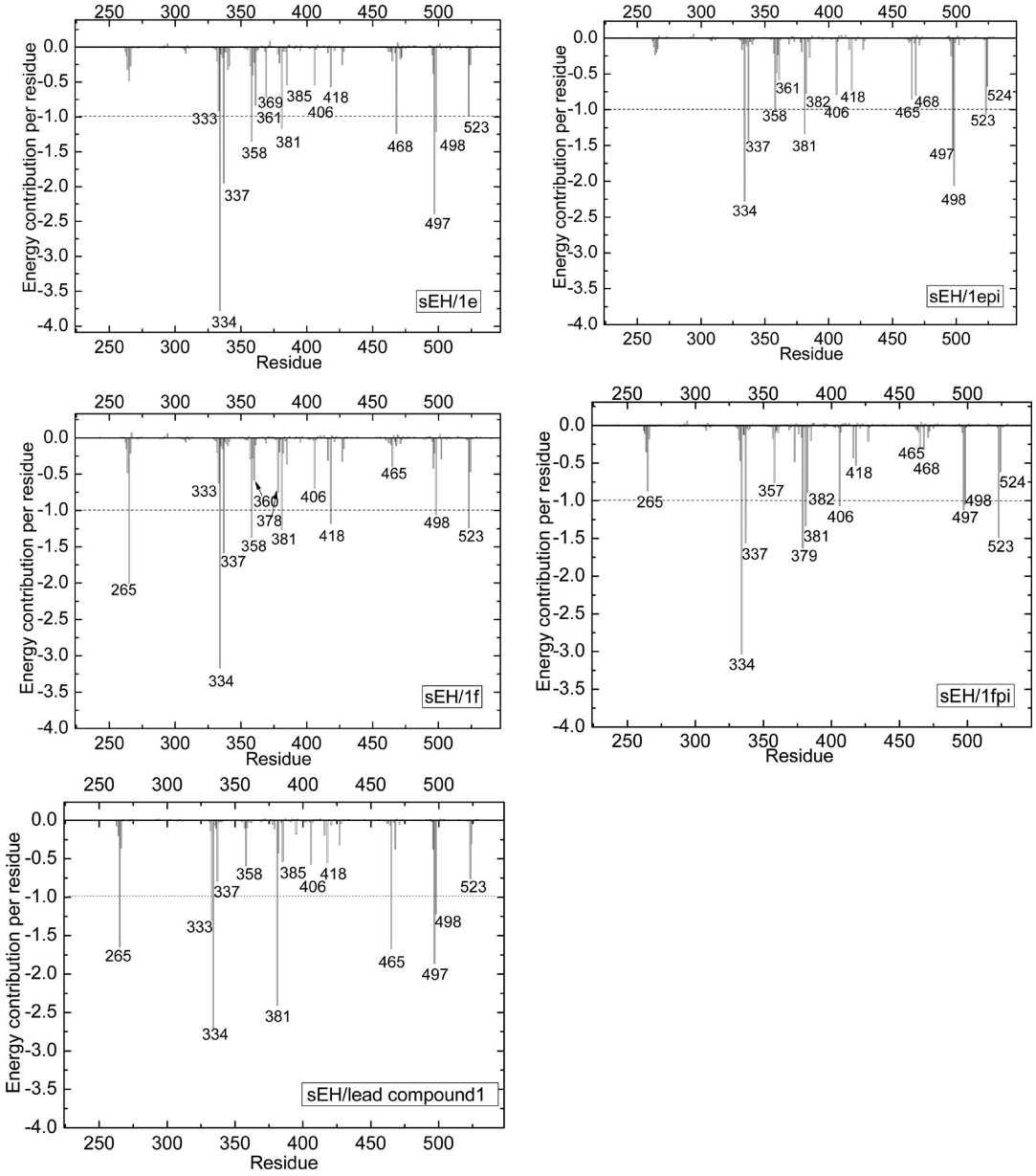

Figure 11. Decomposition of binding free energy on per-residue basis for each protein−inhibitor complex.

Table 4. Binding Free Energies of Two Hydrophobic Pockets (kcal/mol) in Seven Complexes

	sEH/lead compound	sEH/ 1api	sEH/ 1b	sEH/ 1c	sEH/ 1d	sEH/ 1epi	sEH/ 1fpi
larger	−5.96	−9.96	−9.32	−9.66	−9.33	−9.22	−8.7
smaller	−6.73	−5.39	−8.05	−7.79	−6.53	−4.92	−5.35

performed to evaluate their binding affinities. The probable protonation states of histidine in the active site have been ascertained for the crystal structure. The obtained results showed that Hie is the most probable protonation state. According to the calculated results of binding free energies ($\Delta\Delta G_{TOT}$), the overall rank of calculated binding free energies of this set of compounds is in excellent agreement with the rank of experimental IC_{50} values. The correlation coefficient (r^2) between the predicted binding free energies ($\Delta\Delta G_{TOT}$) and experimental bioactivity data (IC_{50}) is 0.88. Further decomposition of the overall binding free energy into some basic components indicates that the van der Waals energies are the dominant component of the total energies, and the entropy changes play an indispensable role in determining the binding free energies of these compounds.

The structural analysis and decomposition of the binding free energy on a per-residue show that all the inhibitors are stabilized by hydrogen bonds and hydrophobic interactions. The conserved hydrogen bonds anchor the inhibitors to the exact site for binding with sEH. The superposition of the average structure of the sEH/lead compound, sEH/1api, sEH/1b, sEH/1c, sEH/1d, sEH/1epi, and sEH/1fpi suggests that all six inhibitors undergo little movements and rotations relative to the lead compound. It gives rise to a different binding mode and interaction mechanism between inhibitor and protein comparing with experimental crystal structure. First, the van der Waals interaction increases after substitution of the cyclopentyl group in the larger hydrophobic pocket and therefor promotes combination of inhibitor. Second, the strength of the hydrogen bond between the nitrogen atom or the oxygen atom of the

dx.doi.org/10.1021/jp304736e | J. Phys. Chem. B 2012, 116, 10219−10233

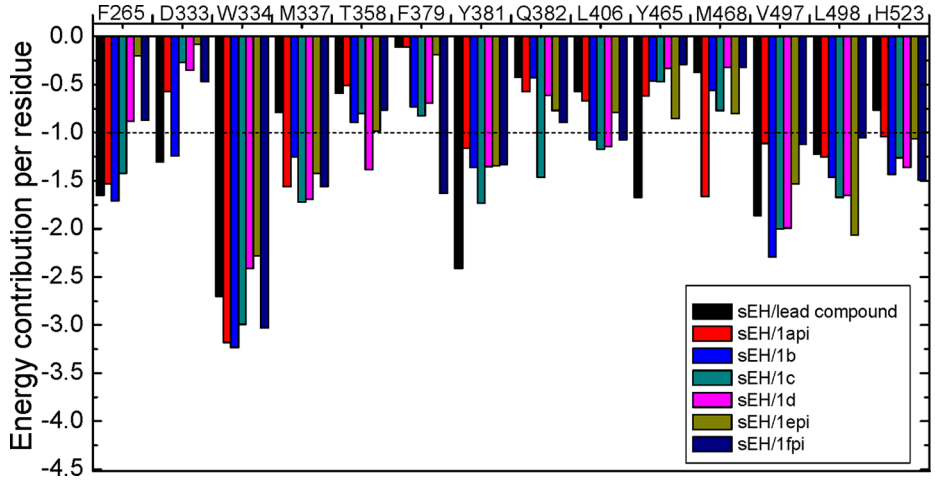

Figure 12. Comparison of interaction energy based on the key residues in the seven sEH/inhibitor complexes.

benzoxazole and Tyr465 is decreased in the smaller pocket as compared with that of the sEH/lead compound complex. In order to avoid steric clash with residue Hie523, 7-methyl has an analogous orientation to 4-methyl of the sEH/1epi complex. Finally, the hydrophobic interactions between ligands and residues play a more important role for association than the hydrogen bond does. Especially, our calculated results reflect that the key residue Trp334 dominates the most binding free energies among all residues. The different potency of these designed inhibitors mainly derives from the van der Waals interaction. The activities of these compounds to the sEH protein are not decided by a certain residue but the common effect of multiple side chains in the binding pocket. The information obtained from this study will be valuable not only for obtaining binding modes and inhibition mechanisms but also for future rational design of novel and more potent sEH inhibitors to treat hypertension and dysglycemia.

■ ASSOCIATED CONTENT

Supporting Information

Comparison between monomer model and homodimer model during MD simulation. This material is available free of charge via the Internet at http://pubs.acs.org.

■ AUTHOR INFORMATION

Corresponding Author

*Fax: +86-551-5141078. E-mail: jghan@ustc.edu.cn.

Notes

The authors declare no competing financial interest.

■ ACKNOWLEDGMENTS

This work is supported by Natural Scientific Fund of China (11179035) and 973 fund of Chinese Ministry of Science and Technology (2010CB934504). Experiments have been performed partly on the Supercomputing Center of University of Science and Technology of China.

■ REFERENCES

(1) Spector, A. A.; Fang, X.; Snyder, G. D.; Weintraub, N. L. *Prog. Lipid Res.* **2004**, *43*, 55−90.
(2) Newman, J. W.; Morisseau, C.; Hammock, B. D. *Prog. Lipid Res.* **2005**, *44*, 1−51.
(3) Yu, Z.; Xu, F.; Huse, L. M.; Morisseau, C.; Draper, A. J.; Newman, J. W.; Parker, C.; Graham, L.; Engler, M. M.; Hammock, B. D.; et al. *Circ. Res.* **2000**, *87*, 992−998.
(4) Schmelzer, K. R.; Kubala, L.; Newman, J. W.; Kim, I.; Eiserich, J. P.; Hammock, B. D. *Proc. Natl. Acad. Sci. U.S.A.* **2005**, *102*, 9772−9777.
(5) Node, K.; Huo, Y.; Ruan, X.; Yang, B.; Spiecker, M.; Ley, K.; Zeldin, D. C.; Liao, J. K. *Science* **1999**, *285*, 1276−1279.
(6) Iliff, J. J.; Alkayed, N. J. *Future Neurol.* **2009**, *4*, 179−199.
(7) Dhanasekaran, A.; Gruenloh, S. K.; Buonaccorsi, J. N.; Zhang, R.; Gross, G. J.; Falck, J. R.; Patel, P. K.; Jacobs, E. R.; Medhora, M. *Am. J. Physiol.: Heart Circ. Physiol.* **2008**, *294*, H724−H735.
(8) Katragadda, D.; Batchu, S. N.; Cho, W. J.; Chaudhary, K. R.; Falck, J. R.; Seubert, J. M. *J. Mol. Cell. Cardiol.* **2009**, *46*, 867−875.
(9) Yousif, M. H. M.; Benter, I. F.; Roman, R. J. *Auton. Autacoid Pharmacol.* **2009**, *29*, 33−41.
(10) Xu, D.; Li, N.; He, Y.; Timofeyev, V.; Lu, L.; Tsai, H.; Kim, I.; Tuteja, D.; Mateo, R. K. P.; Singapuri, A.; et al. *Proc. Natl. Acad. Sci. U.S.A.* **2006**, *103*, 18733−18738.
(11) Sudhahar, V.; Shaw, S.; Imig, J. D. *Curr. Med. Chem.* **2010**, *17*, 1181−1190.
(12) Zeldin, D. C.; Kobayashi, J.; Falck, J. R.; Winder, B. S.; Hammock, B. D.; Snapper, J. R.; Capdevila, J. H. *J. Biol. Chem.* **1993**, *268*, 6402−6407.
(13) Zeldin, D. C.; Wei, S. Z.; Falck, J. R.; Hammock, B. D.; Snapper, J. R.; Capdevila, J. H. *Arch. Biochem. Biophys.* **1995**, *316*, 443−451.
(14) Zeldin, D. C. *J. Biol. Chem.* **2001**, *276*, 36059−36062.
(15) Roman, R. J. *Physiol. Rev.* **2002**, *82*, 131−185.
(16) Ingraham, R. H.; Gless, R. D.; Lo, H. Y. *Curr. Med. Chem.* **2011**, *18*, 587−603.
(17) Imig, J. D. *Cardiovasc. Drug Rev.* **2006**, *24*, 169−188.
(18) Qiu, H.; Li, N.; Liu, J.; Harris, T. R.; Hammock, B. D.; Chiamvimonvat, N. *Cardiovasc. Ther.* **2011**, *29*, 99−111.
(19) Imig, J. D.; Hammock, B. D. *Nat. Rev. Drug Discovery* **2009**, *8*, 794−805.
(20) Fang, X. *Recent Pat. Cardiovasc. Drug Discovery* **2006**, *1*, 67−72.
(21) Anandan, S.; Webb, H. K.; Chen, D.; Wang, Y. J.; Aavula, B. R.; Cases, S.; Cheng, Y.; Do, Z. N.; Mehra, U.; Tran, V.; et al. *Bioorg. Med. Chem. Lett.* **2011**, *21*, 983−988.
(22) Kim, I.; Park, Y.; Hammock, B. D.; Nishi, K. *J. Med. Chem.* **2011**, *54*, 1752−1761.
(23) Eldrup, A. B.; Soleymanzadeh, F.; Farrow, N. A.; Kukulka, A.; De Lombaert, S. *Bioorg. Med. Chem. Lett.* **2010**, *20*, 571−575.
(24) Shen, H. C. *Expert Opin. Ther. Pat.* **2010**, *20*, 941−956.
(25) Morisseau, C.; Goodrow, M. H.; Dowdy, D.; Zheng, J.; Greene, J. F.; Sanborn, J. R.; Hammock, B. D. *Proc. Natl. Acad. Sci. U.S.A.* **1999**, *96*, 8849−8854.

(26) Rose, T. E.; Morisseau, C.; Liu, J.; Inceoglu, B.; Jones, P. D.; Sanborn, J. R.; Hammock, B. D. *J. Med. Chem.* **2010**, *53*, 7067−7075.
(27) Huang, S.; Cao, B.; Morisseau, C.; Jin, Y.; Hammock, B. D.; Long, Y. *MedChemComm* **2012**, *3*, 379−384.
(28) Shen, H. C.; Ding, F.; Deng, Q.; Xu, S.; Tong, X.; Zhang, X.; Chen, Y.; Zhou, G.; Pai, L.; Alonso-Galicia, M.; et al. *Bioorg. Med. Chem. Lett.* **2009**, *19*, 5716−5721.
(29) Chen, D.; Whitcomb, R.; MacIntyre, E.; Tran, V.; Do, Z. N.; Sabry, J.; Patel, D. V.; Anandan, S. K.; Gless, R.; Webb, H. K. *J. Clin. Pharmacol.* **2012**, *52*, 319−328.
(30) Xing, L.; McDonald, J. J.; Kolodziej, S. A.; Kurumbail, R. G.; Williams, J. M.; Warren, C. J.; O Neal, J. M.; Skepner, J. E.; Roberds, S. L. *J. Med. Chem.* **2011**, *54*, 1211−1222.
(31) Singh, D.; Tripathi, A.; Kumar, G. *Nepal J. Biotechnol.* **2012**, *2*, 53−61.
(32) Kubinyi, H. *Curr. Opin. Drug Discovery Dev.* **1998**, *1*, 4−15.
(33) Alonso, H.; Bliznyuk, A. A.; Gready, J. E. *Med. Res. Rev.* **2006**, *26*, 531−568.
(34) Hao, M.; Li, Y.; Wang, Y.; Yan, Y.; Zhang, S. *J. Chem. Inf. Model.* **2011**, *51*, 2560−2572.
(35) AbdulHameed, M. D. M.; Hamza, A.; Zhan, C. *J. Phys. Chem. B* **2006**, *110*, 26365−26374.
(36) Ertl, P. *JME Molecular Editor*; http://davapc1.bioch.dundee.ac.uk/prodrg/jme_window.html.
(37) Schuttelkopf, A. W.; van Aalten, D. M. F. *Acta Crystallogr., Sect. D: Biol. Crystallogr.* **2004**, *60*, 1355−1363.
(38) Frisch, M. J.; Trucks, G. W.; Schlegel, H. B.; Scuseria, G. E.; Robb, M. A.; Cheeseman, J. R.; Montgomery, J. A., Jr.; Vreven, T.; Kudin, K. N.; Burant, J. C.; Millam, J. M.; Iyengar, S. S.; Tomasi, J.; Barone, V.; Mennucci, B.; Cossi, M.; Scalmani, G.; Rega, N.; Petersson, G. A.; Nakatsuji, H.; Hada, M.; Ehara, M.; Toyota, K.; Fukuda, R.; Hasegawa, J.; Ishida, M.; Nakajima, T.; Honda, Y.; Kitao, O.; Nakai, H.; Klene, M.; Li, X.; Knox, J. E.; Hratchian, H. P.; Cross, J. B.; Bakken, V.; Adamo, C.; Jaramillo, J.; Gomperts, R.; Stratmann, R. E.; Yazyev, O.; Austin, A. J.; Cammi, R.; Pomelli, C.; Ochterski, J. W.; Ayala, P. Y.; Morokuma, K.; Voth, G. A.; Salvador, P.; Dannenberg, J. J.; Zakrzewski, V. G.; Dapprich, S.; Daniels, A. D.; Strain, M. C.; Farkas, O.; Malick, D. K.; Rabuck, A. D.; Raghavachari, K.; Foresman, J. B.; Ortiz, J. V.; Cui, Q.; Baboul, A. G.; Clifford, S.; Cioslowski, J.; Stefanov, B. B.; Liu, G.; Liashenko, A.; Piskorz, P.; Komaromi, I.; Martin, R. L.; Fox, D. J.; Keith, T.; Al-Laham, M. A.; Peng, C. Y.; Nanayakkara, A.; Challacombe, M.; Gill, P. M. W.; Johnson, B.; Chen, W.; Wong, M. W.; Gonzalez, C.; Pople, J. A. *Gaussian 03*, revision B.01; Gaussian, Inc.: Wallingford, CT, 2003.
(39) Huey, R.; Morris, G. M.; Olson, A. J.; Goodsell, D. S. *J. Comput. Chem.* **2007**, *28*, 1145−1152.
(40) Gomez, G. A.; Morisseau, C.; Hammock, B. D.; Christianson, D. W. *Protein Sci.* **2006**, *15*, 58−64.
(41) Argiriadi, M. A.; Morisseau, C.; Hammock, B. D.; Christianson, D. W. *Proc. Natl. Acad. Sci. U.S.A.* **1999**, *96*, 10637−10642.
(42) Argiriadi, M. A.; Morisseau, C.; Goodrow, M. H.; Dowdy, D. L.; Hammock, B. D.; Christianson, D. W. *J. Biol. Chem.* **2000**, *275*, 15265−15270.
(43) Gomez, G. A.; Morisseau, C.; Hammock, B. D.; Christianson, D. W. *Biochemistry* **2004**, *43*, 4716−4723.
(44) Sanner, M. F. *J. Mol. Graphics Modell.* **1999**, *17*, 57−61.
(45) Morris, G. M.; Huey, R.; Lindstrom, W.; Sanner, M. F.; Belew, R. K.; Goodsell, D. S.; Olson, A. J. *J. Comput. Chem.* **2009**, *30*, 2785−2791.
(46) Pettersen, E. F.; Goddard, T. D.; Huang, C. C.; Couch, G. S.; Greenblatt, D. M.; Meng, E. C.; Ferrin, T. E. *J. Comput. Chem.* **2004**, *25*, 1605−1612.
(47) Garriga, M.; Caballero, J. *Chemosphere* **2011**, *82*, 1604−1613.
(48) Case, D. A.; Darden, T. A.; Cheatham, I.; Simmerling, C. L.; Wang, J.; Duke, R. E.; Luo, R.; Crowley, M.; Walker, R. C.; Zhang, W. et al. *AMBER*; University of California: San Francisco, CA, 2008.
(49) Duan, Y.; Wu, C.; Chowdhury, S.; Lee, M. C.; Xiong, G.; Zhang, W.; Yang, R.; Cieplak, P.; Luo, R.; Lee, T.; et al. *J. Comput. Chem.* **2003**, *24*, 1999−2012.
(50) Lee, M. C.; Duan, Y. *Proteins* **2004**, *55*, 620−634.
(51) Wang, J.; Wolf, R. M.; Caldwell, J. W.; Kollman, P. A.; Case, D. A. *J. Comput. Chem.* **2004**, *25*, 1157−1174.
(52) Jorgensen, W. *J. Chem. Phys.* **1983**, *79*, 926.
(53) Darden, T.; York, D.; Pedersen, L. *J. Chem. Phys.* **1993**, *98*, 10089−10092.
(54) Ryckaert, J.; Ciccotti, G.; Berendsen, H. J. C. *J. Comput. Phys.* **1977**, *23*, 327−341.
(55) Feig, M. *J. Chem. Phys.* **2004**, *120*, 903.
(56) Kollman, P. A.; Massova, I.; Reyes, C.; Kuhn, B.; Huo, S.; Chong, L.; Lee, M.; Lee, T.; Duan, Y.; Wang, W.; et al. *Acc. Chem. Res.* **2000**, *33*, 889−897.
(57) Case, D. A.; Cheatham, T. E.; Darden, T.; Gohlke, H.; Luo, R.; Merz, K. M.; Onufriev, A.; Simmerling, C.; Wang, B.; Woods, R. J. *J. Comput. Chem.* **2005**, *26*, 1668−1688.
(58) Onufriev, A.; Bashford, D.; Case, D. A. *Proteins* **2004**, *55*, 383−394.
(59) Weiser, J.; Shenkin, P. S.; Still, W. C. *J. Comput. Chem.* **1999**, *20*, 217−230.
(60) Gohlke, H.; Kiel, C.; Case, D. A. *J. Mol. Biol.* **2003**, *330*, 891−913.